Relative Influences of Cracking and Connection Yield on Transverse Distributions of Moments and Reactions in Timber-Concrete Composites

J. Mudie [1*], W. M. Sebastian [2], J. Norman [1], I. P. Bond [1]

[1] School of Civil, Aerospace, and Mechanical Engineering, University of Bristol, University Walk, Bristol, BS8 1TR, UK

[2] Dept of Civil, Environmental & Geomatic Engineering, University College London, Chadwick Building, Gower St, London, WC1E 6BT, UK

ABSTRACT: This paper uses tests backed up by nonlinear FE analysis for parametric study of transverse load sharing in timber-concrete composites (TCCs) comprising hardwood LVL joists and ductile steel mesh connectors. The results show that while cracking had little effect on transverse distribution of midspan moments, it did change the transverse distribution of reactions by a factor of up to 1.55. Conversely, connection yield had little effect on reactions, but it changed the transverse distribution of midspan moments by a factor up to 1.5. Further, the test-verified FE analyses revealed that an inadvertent 20% drop in concrete tensile strength observed in the tests exacerbated support reaction sharing by up to 15%. These numbers encroach on the load safety factors used in design. Wider studies are needed to determine practical bounds for these load sharing effects and to develop user-friendly means of allowing for these effects in design.

KEYWORDS: timber concrete composite; indeterminacy; experiment; transverse distribution; load sharing; nonlinear; FEA; hardwood; LVL

[*] Corresponding author email address: joshua.mudie@bristol.ac.uk

1 Introduction

1.1 Literature Review

A timber-concrete composite construction comprises a timber joist overlain by a concrete slab, mechanically connected together to inhibit longitudinal slip between the two components. The principle of TCC structural behaviour lies in the assumption that, in a simply-supported beam, the slab will be mostly in compression, and the joist mostly in tension, exploiting the complementary stress resisting properties of the concrete and timber respectively [j]. In practice, slip occurs at the material interface due to the longitudinal shear flexibility of the timber-concrete connectors, and therefore the cross-section experiences a reduced stiffness compared to a fully-composite section [n]. The effectiveness of connectors can be represented by a "connector efficiency" [b, c], which compares the effective stiffness of the section using the specified shear connectors, to that of using rigid connectors.

The options available to achieve high levels of connection efficiency are notched, glued, and mesh plate connections. The notched connection is generally very stiff (stiffness of >0.3-0.5kN/mm per mm of notch) due to interlocking of the concrete slab and timber joist [o]. Vertical screws passing through holes in the slab and threaded into the timber resist vertical separation [l], enhance slip stiffness and provide ductility in the connection [j].

Glued connections exhibit near 100% connection efficiency [k], albeit with reduced ductility once the connection itself has reached its longitudinal shear strength. These glued connections can vary, from bonding a timber joist to a pre-cast concrete slab [k], or casting fresh concrete onto a timber joist with an adhesive already applied that bonds with both the timber and the concrete during the concrete curing process [a]. A relatively recent innovation in timber-concrete shear connectors is the expanded steel mesh connector, which exhibits in general a high stiffness (above 1.0kN/mm per mm of connector), followed by a significant ductility plateau [g, h]. As an example the proprietary HBV connector has been developed and used in various research and construction projects [h, i].

Due to the connection of the two components within the structure, all TCCs are internally indeterminate. Few studies to date have investigated the potentially beneficial effects of external indeterminacy in TCC specimens. One study experimentally investigated the behaviour of longitudinally indeterminate (continuous) TCC T-beams using partially-threaded (PT) and fully-threaded (FT) screws [p]. Load cell recordings showed that the intermediate support reactions for the TCC beams varied in a distinctly nonlinear manner at higher loads. Consequently, relative to a uniform propped cantilever, the PT TCC beam exhibited 0%, 22%, and 61% redistribution of the intermediate support reaction at 29%, 88%, and 100% respectively of its failure load.

Turning now to transversely indeterminate TCC floor systems, the two primary metrics that define the load sharing across such a system are support reaction distribution and midspan bending moment distribution. Monteiro et al. [d] conducted a comprehensive experimental and predictive investigation into the load responses of five-joist TCC floor specimens combining GL24h glulam and vertical dowel connections, with the intention of gaining a better understanding of transverse load sharing, utilising support reaction sharing as the descriptor for load distribution. Some of the key features of and conclusions from the study are:

- A five-joist arrangement allowed for investigation of full load distribution, and identification of the attenuation of load sharing at distance from the point of loading. Strain measurements indicated that the loaded joist may only effectively transfer load to two adjacent joists on each side, when a joist spacing of 600mm is used.
- A combination of concentrated and line loading provided insight into the effects that these different loading arrangements have on load distribution in TCC floors and provide real-world context. A concentrated load above the central joist resulted in a midspan deflection 71% larger than that of an equivalent line load.
- Different spans and geometric characteristics were altered to gain a broad insight into the behaviour of the floors. A 2m span was 35% less effective at transversely sharing load than a 4m or 6m span. A thinner slab (30mm, down from 50mm) and use of lightweight concrete (75% density of normal weight concrete) also reduced the ability of the specimen to transfer loads, but by a lesser extent (5% and 10% respectively for central joist loaded)

In addition to the work by Monteiro et al., investigations into transverse load sharing have also been conducted by Kieslich and Holschemacher [e], who focused on three-joist floor specimens which combined glulam joists with 120mm timber screws, vertically inserted into the joists. The extent of load distribution was ascertained via the supposition that midspan deflections are directly proportional to load sharing. The results suggest that at loads which cause a maximum joist deflection of span/300, the deflection of the outer joists is 79.7% that of the centre joist, for the normal concrete specimen at 750mm joist spacing. The influence of a lightweight concrete reduced this value to between 66.4% and 76.8%. On the effect of the transverse span of the slab across the joists, a joist spacing of 900mm (increased from 750mm) decreased this deflection ratio to 61.1% (from 66.4%), and a reduction to 600mm spacing (again, from 750mm) increased the ratio to 82.2% (again, from 66.4%), highlighting that more closely spaced joists result in better transverse load sharing.

Mudie et al. [f] built on the above works [d, e] by also investigating another crucially important metric to assess load sharing, namely the midspan bending moment distributions, and by investigating both the support reaction sharing and the midspan moment sharing metrics from zero load up to failure, not just within the elastic regime. This study was the first to use the combination of hardwood beech LVL and expanded steel mesh connectors to investigate the phenomenon of load sharing within a multi-joist (in this case three-joist) TCC structure. Benefits of this combination include the high stiffness, strength and ductility of the connections coupled with the high stiffness and strength of the hardwood. The load-induced moments were inferred for a full-scale TCC floor specimen using data from an ad-hoc arrangement of strain gauges at multiple elevations throughout the specimen depth. Under a concentrated load applied to the slab at midspan directly above the middle of the three joists, the work presented in Mudie et al. [f] highlighted a number of important results, namely:

- Support reaction sharing and midspan moment sharing were palpably different from each other (reaching a maximum difference of 20.7% at 75% of maximum load) – meaning that it is not sufficient to simply measure support reaction sharing as a proxy for midspan moment sharing;
- In progressing from zero load to failure, the moment share for the central TCC T-section varied between 42.5% and 51.3%, highlighting that this value was not a constant, but rather seemed

to have been a function of concrete cracking and progressive nonlinearity of the shear connections with increase of the applied load.

- The expanded steel mesh plate connector was shown to provide excellent slip stiffness, longitudinal shear strength and ductility, although that ductility was not significantly exploited before the overall floor specimen failed by fracture of the timber joists at midspan.

These results point to a clear need to further widen the body of experimental work that investigates the transverse distributions of both support reactions and midspan moments in multi-joist TCC floors, and to provide further insight into the roles that cracking and connector yield have on influencing these distributions. Moreover, in the above study [f], the potential of the steel mesh connectors remained unfulfilled at ultimate loading, as shown by the lack of activated ductility. It is desirable that these connectors undergo significant plastic deformation before the structure reaches its ultimate load capacity to influence as much as possible a ductile failure of the structure, and as much internal stress redistribution as possible during the failure regime so that the failure load is rendered somewhat predictable. Throughout the remainder of this paper the term ductility will be used in two contexts, namely:

- Local ductility, represented by yield and subsequent slip in the shear connectors;
- Global ductility, represented by the overall load response of the structure and which is influenced by multiple effects including connection yield and concrete cracking.

Given the above discussion, the primary aim of the study reported in the rest of the present paper is to use parallel laboratory tests and finite element analyses to understand the relative influences of cracking and connection yield on the transverse distributions of both midspan moments and support reactions in multi-joist TCCs. One of the laboratory specimens (S1) used for this purpose has been reported on previously [f], and a second, new, specimen (S2) is presented in this paper. Informed by the observations from testing S1 to failure, S2 was equipped with a different layout (relative to S1) of the same steel mesh connectors, to try and draw out more local ductility during the failure regime, giving an opportunity to observe the impact of this ductility on overall load response in the approach to ultimate loading. Alongside the tests, the FE analysis incorporated models for the nonlinear behaviours of the

connections and of the concrete to give further insight into the structural significance of the experimental results.

1.2 Objectives of Present Study

The key objectives of the study reported on in this paper are as follows:

- To understand the relative roles that concrete cracking and connector yield have on the support reaction sharing and bending moment sharing within a TCC;
- To illustrate the extent to which the measured load response is predictable, through the use of state-of-the-art nonlinear finite element analysis (NLFEA);
- To understand the influence of an altered connection layout on TCC load response, including its impact on transverse load sharing capability;
- To use the test-verified FEA for wide parametric study focused on any important variable as observed from the tests.

2 Material and Methods

The fabrication of the experimental specimen S2, used as a comparator in this study, followed the same process as that described by Mudie et al. [f] for specimen S1. The fabrication entailed the grooving of joists and subsequent bonding of connectors. Following this, a formwork was built and a (target RC32/40) concrete slab cast across the joists.

The cross-section and elevations of S1 and S2 are shown in Figure 1. As can be seen, both comprise a concrete slab of 80mm thickness overlaying three hardwood (beech) LVL joists of dimensions 120x200x4900mm. These BauBuche GL70 type S LVL joists were spaced at 700mm centres, and named joist J1, J2, and J3 respectively. An A193 steel reinforcing mesh was positioned at the mid-depth of the slab to inhibit shrinkage cracks during concrete curing. Baubuche X panels of 19 mm thickness, used as permanent formwork given the wet concrete construction, also represented a connection interlayer separating the joists from the slab. A photograph of the specimen ready for testing may be seen in Figure 2.

The primary difference between specimens S1 and S2 is the shear connection distribution. In order to estimate the number of shear connectors required for S1 the following method was adopted: a simple FE grillage model of the three-joist specimen was set up which utilised longitudinal elements to represent the three individual TCC T-sections, and transverse elements to represent the transverse action of the concrete slab. For the longitudinal elements, an effective stiffness calculated using the Eurocode 5 Gamma method approach [m] was applied to each T-section. In the transverse direction, concrete cracking and presence of reinforcing bars was accounted for. A load was applied to the specimen and the support reaction magnitudes provided the maximum shear force, which could then be used to estimate the longitudinal shear flow and therefore the longitudinal shear forces experienced in each connector (determined via the results of push-out tests [f]). Following experimental testing, it was found that the load distribution did not match that of the simplified model, resulting in a lack of ductility in the connectors before reaching maximum load.

For S2, a more refined model was developed which employed separate elements for slab and joist, connected by springs at the centroid of each connector location. This removed the need to infer connector shear forces from support reactions, as the forces in the springs directly defined the longitudinal shear forces in the corresponding connectors. This approach also removed the reliance on the estimated effective section stiffness as the material properties for the timber and concrete, and the load-slip properties of the connector could be individually specified. This model, when placed under the same midspan, mid-joist concentrated loading as for laboratory test specimen S1, suggested that a shear connection layout consisting of five steel mesh connections per joist for specimen S2 (Figure 2c), instead of nine steel mesh connections per joist as for specimen S1 (Figure 2b), would enable significantly more ductility of S2 before maximum load than experienced in the previous specimen S1. Further to this analysis using linear elastic models, a nonlinear FE model was developed to model the specimens in more depth and is presented later in the paper.

158

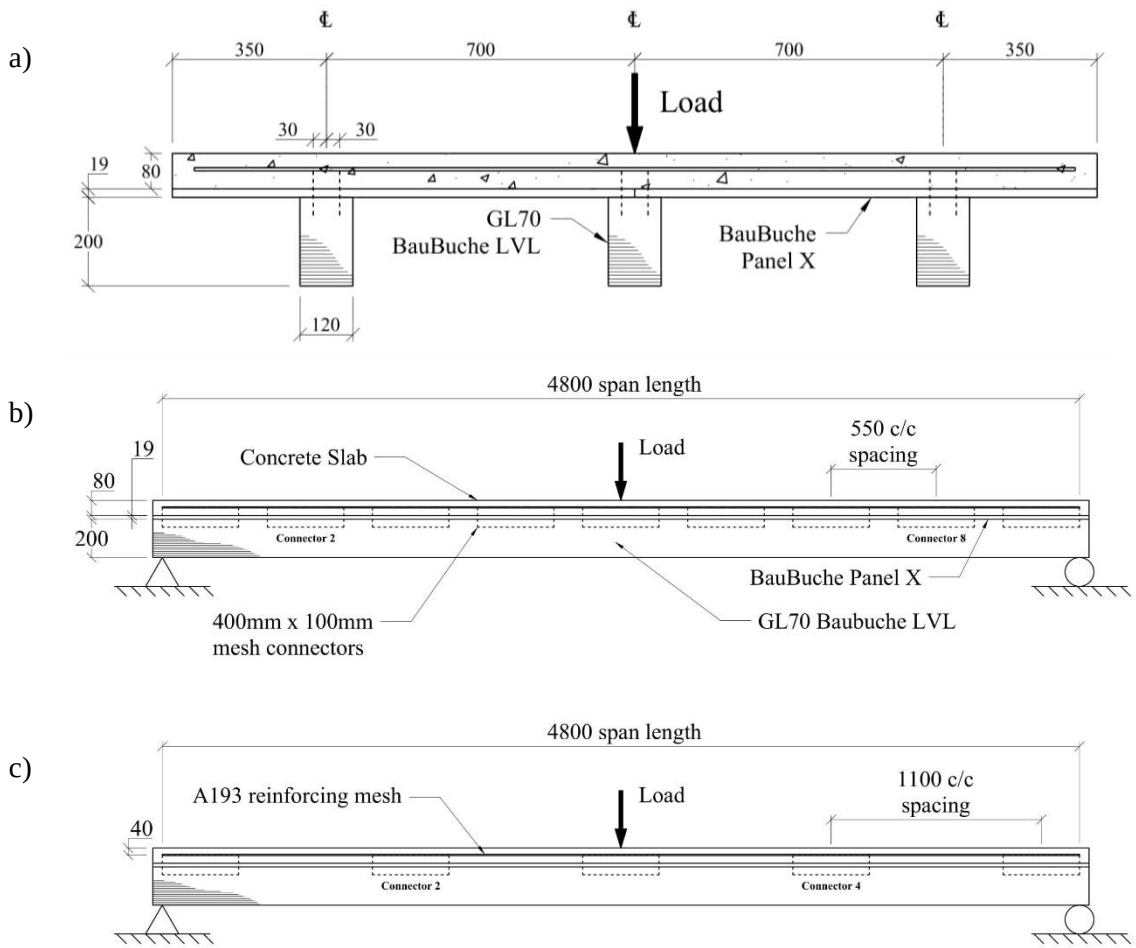

159 *Figure 1 – (a) Cross-section (both specimens), and side elevations of full-scale experimental specimens (b) S1, and (c) S2.*

160

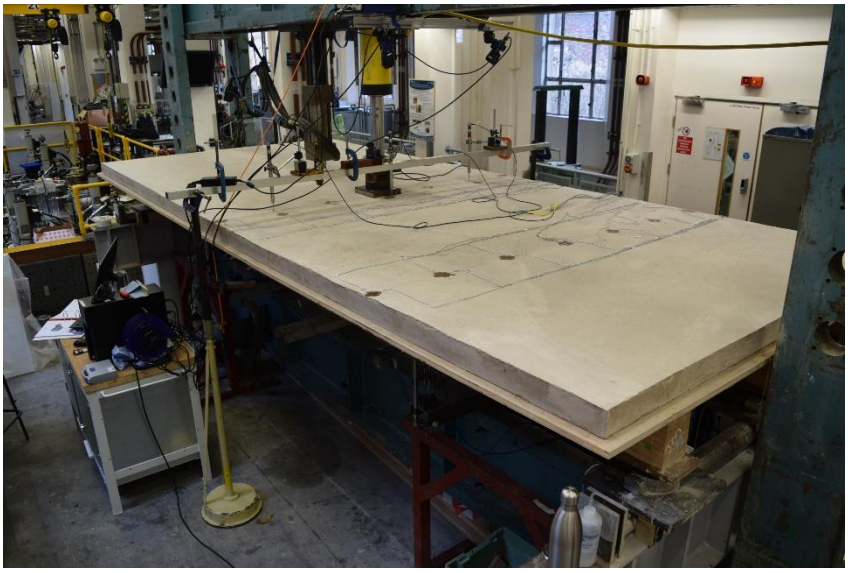

161

162 *Figure 2 - Photo of the full-scale specimen S2 with instrumentation (concrete strain gauges, midspan LVDTs) visible*

163

In addition to the altered connection distribution between the two specimens, there was an additional, unintended, difference between the two specimens, namely the concrete slab properties. Whilst geometrically identical, material tests on concrete cube samples taken from the specimens indicated a discrepancy between the two concrete slabs: the average cube strengths obtained for the S1 and S2 samples were 43.3N/mm^2 and 33.3N/mm^2 respectively. For both S1 and S2, the same RC32/40 mix was specified to and delivered by the same ready-mix concrete supplier. It was noted that the concrete mix delivered for S2 was significantly more watery than that delivered for S1, but the extent of this strength discrepancy was noted only when concrete cube samples were tested. The S2 strength is 23% lower than S1, which is likely to have some impact on the behaviour of the second specimen in comparison to the first, and this is considered in discussing the comparison between the S1 and S2 results. Note also that an average cube compressive strength of 52.9N/mm^2 was obtained for the concrete slabs used in the double shear connection specimens which provided slip stiffness and longitudinal shear strength data for the S1 and S2 designs. Table 1 provides a summary of the concrete strengths for the slabs in S1 and S2, and the respected sides of the double shear test specimens each cast in two stages, one for each slab block component.

Table 1 - Concrete cube compressive strength and coefficient of variation

Concrete Sample	No. cubes tested	Mean compressive strength (N/mm^2)	Coefficient of Variation (N/mm^2)
S1	4	43.3	2.51
S2	3	33.3	5.07
Connections (side 1)	8	52.4	10.74
Connections (side 2)	4	53.3	7.28

2.1 Instrumentation

In order to be able to fulfil the key aims of the paper, namely, to gain a richer understanding of the midspan moment and support reaction sharing in full-scale TCC floors, and to explore the influence of changing the shear connection layout on these and other important facets of multi-joist TCC structural action, strain gauges and load cells were used strategically to enable capture of some crucial data as follows:

- Load cells placed under each support allowed the determining of support reaction distributions across the specimen at both ends (Figure 3a). A load cell placed under the point of applied load enabled equilibrium checks to be carried out to verify the data.
- Strain gauges placed at three elevations through the depth of the joist, on each of the three joists at quarter- and mid-spans, allowed for a through-depth strain distribution of the joists to be determined (Figure 3b). Utilising the assumptions of curvature compatibility and no slip between the concrete and interlayer, but allowing slip through the thickness of the interlayer, a further strain gauge on the top surface of the concrete slab allowed for a full through-depth strain distribution to be obtained for the TCC T-section comprising each LVL joist and its associated width of slab (taken as a third of the full slab width).
- For each such T-section these through-depth strains could then be converted to stresses, forces and moments.
- Slip measurements were taken using linear potentiometers placed between the timber joist and timber interlayer (Figure 3a), again under the assumption that the location of slip is at the timber-interlayer interface as demonstrated by previous connection testing [f]. Five slip gauges were used per joist, spaced equally along the length, at both ends, mid-span and at quarter-spans.
- Deflections at midspan and both quarter spans were measured underneath each joist using an array of nine linear voltage displacement transducers (LVDTs), marked in Figure 3a.

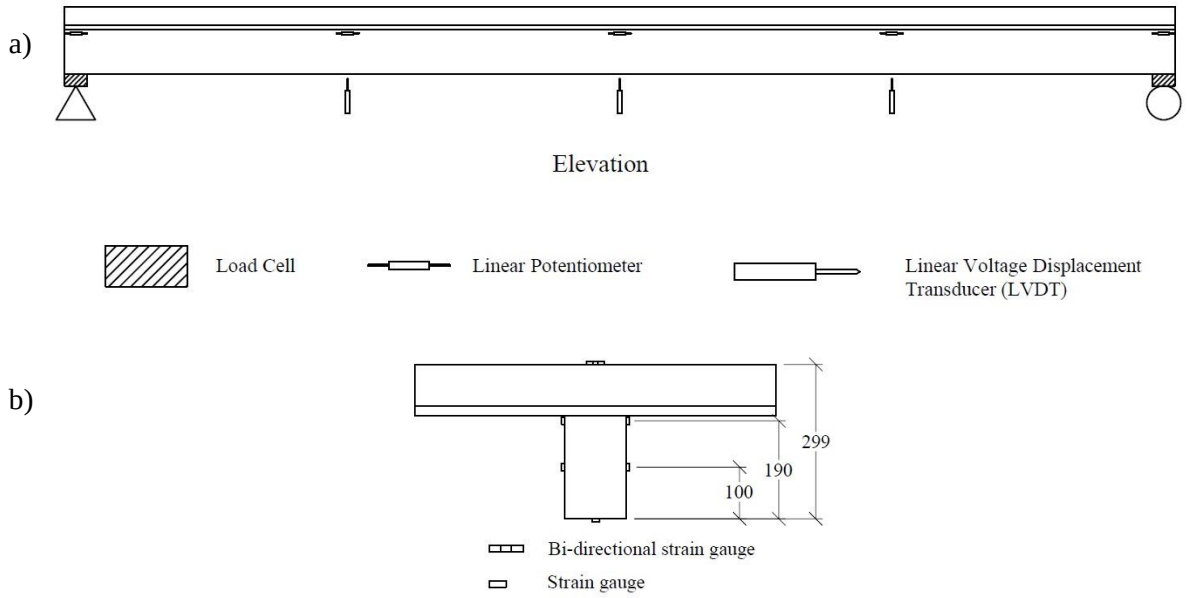

Figure 3 - Instrumentation layout for both specimens comprising (a) load cells, potentiometers, LVDTs, and (b) strain gauge layout at midspan and quarter-span for each TCC T-section

2.2 Testing Regime

Specimen S2 was subjected to several loading magnitudes and arrangements. To fully understand the load sharing of the S2, tests were carried out applying a 20kN point load onto the slab alternately above the centreline of each of the joists J1 to J3 respectively, at midspan, to represent loading within the serviceability limit state (SLS). Following this, a load-to-failure test was carried out with the specimen loaded on the slab directly above the centreline of the central joist J2 at midspan.

3 Load Responses of TCC Specimens with Differing Shear Connection Densities

The key driver behind this paper is the determining of the influence of cracking and connection yield on the transverse distribution of support reactions and midspan moments in TCCs. Before this can happen, it is important to understand the influence that changing the connection layout (in this case density) has on structural behaviour including ductility of full-scale TCC floors To those ends, this section first compares the experimentally observed load responses of specimens S1 and S2, followed by the impact of these responses on support reaction and bending moment distributions, and finally utilising these results along with further analysis to better understand the relative roles of cracking and connection yield on this behaviour. Note here, as mentioned in Section 2, that the compressive strengths of the S1, S2 and connection specimen concretes were different from each other. Hence, the influence of the concrete strength on these results will also be discussed alongside the important impacts of the shear connector distributions. For reference, Figure 4 presents the shear force vs. slip curves for the four double-shear test specimens [f] which were used to determine the expanded mesh connection properties.

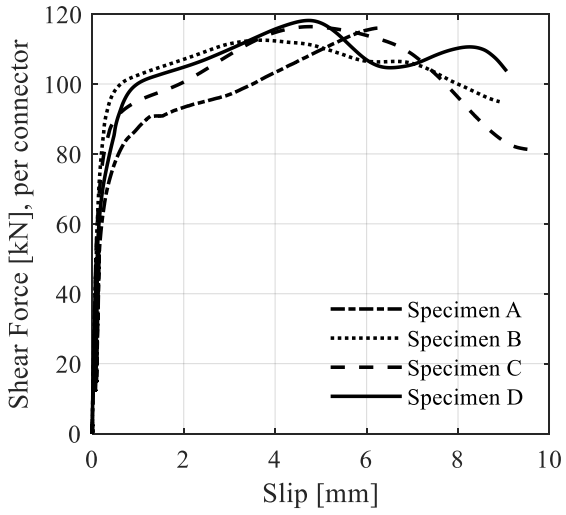

Figure 4 - Shear force vs. slip relationship of the expanded mesh plate connectors, derived from double shear testing [f]

3.1 Specimen Behaviour and Ductility

Figure 5 compares the load vs. central deflection behaviours, and joist-interlayer slip between specimens S1 and S2. Also included in Figure 5a are the stages at which, during testing, loud bangs were heard, leading to the discontinuities seen. None of these bangs represented the final failure of the specimens which happened shortly after the end of both plots. Whilst the causes of these bangs are uncertain, it is evident that they coincided with the discontinuities on the plots, indicating that there may have been occurrences such as concrete cracking (pre-yield) or connector bond failure (post-yield). The differences between the two plots of Figure 5 may be summarised as follows:

- *Initial Gradient:* Despite the significant difference in concrete strength, the initial gradient of the load-deflection response is not too dissimilar between S1 and S2. This indicates that the influence of the lower-strength concrete on the initial behaviour is minimal. When comparing these gradients for S1 and S2 (7.93kN/mm and 6.70kN/mm respectively) the difference of 18% matches closely with the percentage difference in effective section stiffness (EI_{eff}) calculated using the Gamma method as described in Annex B of Eurocode 5 [m] (8.08×10^{12} Nmm^2 vs. 7.04×10^{12} Nmm^2, a difference of 15%), using the elastic moduli for the concrete strengths as measured. The influence of the concrete constitutive behaviour is not pronounced because the difference in concrete modulus (estimated as 3kN/mm^2 according to Eurocode 2 [q]) is modest despite the significant change in cube strength (10N/mm^2) between S1 and S2.
- *Interaction Between Local and Global Yield*: Figure 5b, by reference to Figure 4, shows that first yield of the connections, a local manifestation of ductility, occurred at 156 kN and 78 kN for S1 and S2 respectively. Coincidentally, Figure 5a shows that at those same loads, an abrupt and significant lowering of the tangent stiffness occurred, which is a global manifestation of ductility. Hence localised ductility within the spatially concentrated mesh connectors triggered global ductility of the entire structure.
- *Self-Consistency of Test Data on First Yield*: For the first yield loads on Figure 5a as just described above, the test-recorded load cell readings from the middle joist (J2) supports were

entered into the beam theory formula for longitudinal shear force at the joist-slab interface. This led to predicted support forces of 121 kN and 124 kN for S1 and S2 respectively. Comparison with Figure 4, and noting that the connection forces might be slightly less than the 121-124 kN values owing to longitudinal shear transfer along the middle T-section's slab edges, again point to yield of the connections. This approach of using some of the test data (load cell recordings) to independently verify a point made by other facets of the test data (load, deflection and slip recordings), points to the self-consistency of the test results.

- *Post-yield line:* By examining the gradients of the respective applied load vs. deflection plots after first yield, it is possible to understand the level of global ductility that the specimens exhibited: as mentioned previously S1 had an average initial stiffness of 7.93kN/mm, reducing to 1.24kN/mm after yield. Comparing this with S2, the initial stiffness is similar at 6.70kN/mm, but reduces significantly to 0.70kN/mm after yield. This reduction of almost 90% in stiffness highlights the close approximation to ductile behaviour exhibited by S2. The stiffness loss in S1 is still large – an 84% reduction is experienced after connector yield. Combined with the increased deflection magnitude after yield, this suggests that the presently reduced connection density has had an appreciable impact on the global ductility of the present multi-joist TCC specimens. Finally, note that the plastic (first yield to peak load)-to-elastic deflection ratio is

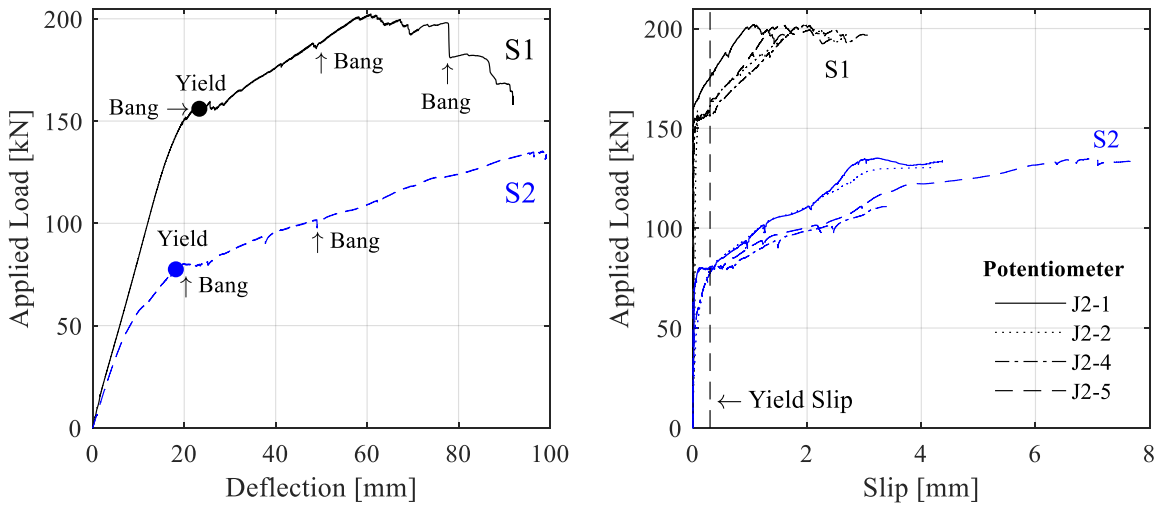

Figure 5 – S1 and S2 results compared: (a) Load vs. J2 midspan deflection; (b) Variation with load of slip at different locations along J2

4.6 and 1.69 for S2 and S1 respectively, indicating that the reduced slab-joist connectivity led to a proportionally much larger elasto-plastic regime for S2.

3.2 Bending Moment and Support Reaction Distribution

The Multi-Layer Analysis (MLA) tool first presented in a previous study [f], was employed to convert the recorded through-depth strains to TCC T-section moments, as described earlier in Section 2.1 of the present paper. This enabled quantification of the midspan moment sharing. In addition, the load cell data recorded from the tests were used to establish the support reaction sharing across the specimens. These two datasets help to fully understand the impact of altered connection layouts on transverse distribution across TCC specimens.

Figure 6a shows the support reaction share taken by J2 for the tests on S1 and S2. Note that for S1, two pre-loads of 100kN and 125 kN (both in the pre-yield regime) were applied which are represented in the figure by the dashed lines. Figure 6a shows that these loads of 50% and 62.5% of maximum load had an appreciable impact on the structural behaviour of the specimen, with the outer joists shedding load back to the central joist at a faster rate in each test, indicating that significant nonlinear behaviour was being experienced above 50kN, and that non-recoverable damage was being done to the specimen in each of these tests. This highlights that nonlinearity in the transverse distribution occurred *before* the connector yield identified in Figure 5, suggesting a change of internal stiffness profile (possibly due to cracking) in the concrete slab might have led to this behaviour. It was intended that the second specimen would be subjected to the same “proof loads” of 100kN and 125kN, but due to the significant observed load shift towards the centre joist J2 the specimen was loaded directly to failure, as the proximity to failure was seen to be much closer.

Comparing the initial dashed line for S1 and experimental line for S2 the profiles are more similar than for the final 200kN test. Despite this, it is clear to see that there is a marked difference in the behaviour of the two specimens: S1 experiences a sharp decrease in support reaction sharing after 65kN, from a 49% load distribution to 40% with an additional 47kN applied load. Comparing this to S2 the difference

is even more palpable, with a reduction in load distribution of 27% between 45kN and 80kN applied load.

The majority of the shifting in the support reactions occurs before the yield point of the connections, identified in Figure 5. Therefore, it may be assumed that for *both specimens* this initial support reaction shifting was not due to connection ductility, but due to a change of internal stiffness profile, potentially manifested through concrete cracking. The gradient of this shift is therefore likely a function of the concrete strength, which for S2 was demonstrably lower, as described previously. If the connector yield is seen to happen at the locations described, then it can be posited that these specific full-scale TCC specimens underwent three key stages of behaviour, namely a linear elastic period of deformation, followed by nonlinearity governed by the reduction of transverse stiffness (potentially due to concrete slab cracking), and subsequently loss of longitudinal stiffness due to connector yield.

Figure 6b shows the bending moment share of J2, using the same axis scale to better show the comparison between the two. Two things are clear from the outset:

- The bending moment sharing is consistently more favourable than the support reaction sharing, especially towards the higher end of the loading regime, where for S1 the J2 support reaction share reached 67% compared to 52% moment share, while for S2 the support reaction share reached a maximum of 74% compared to 59% for moment share.
- Transverse moment distribution was far less influenced by load history than was transverse distribution of support reactions. The reason for this is currently unclear and requires further investigation in a future study.

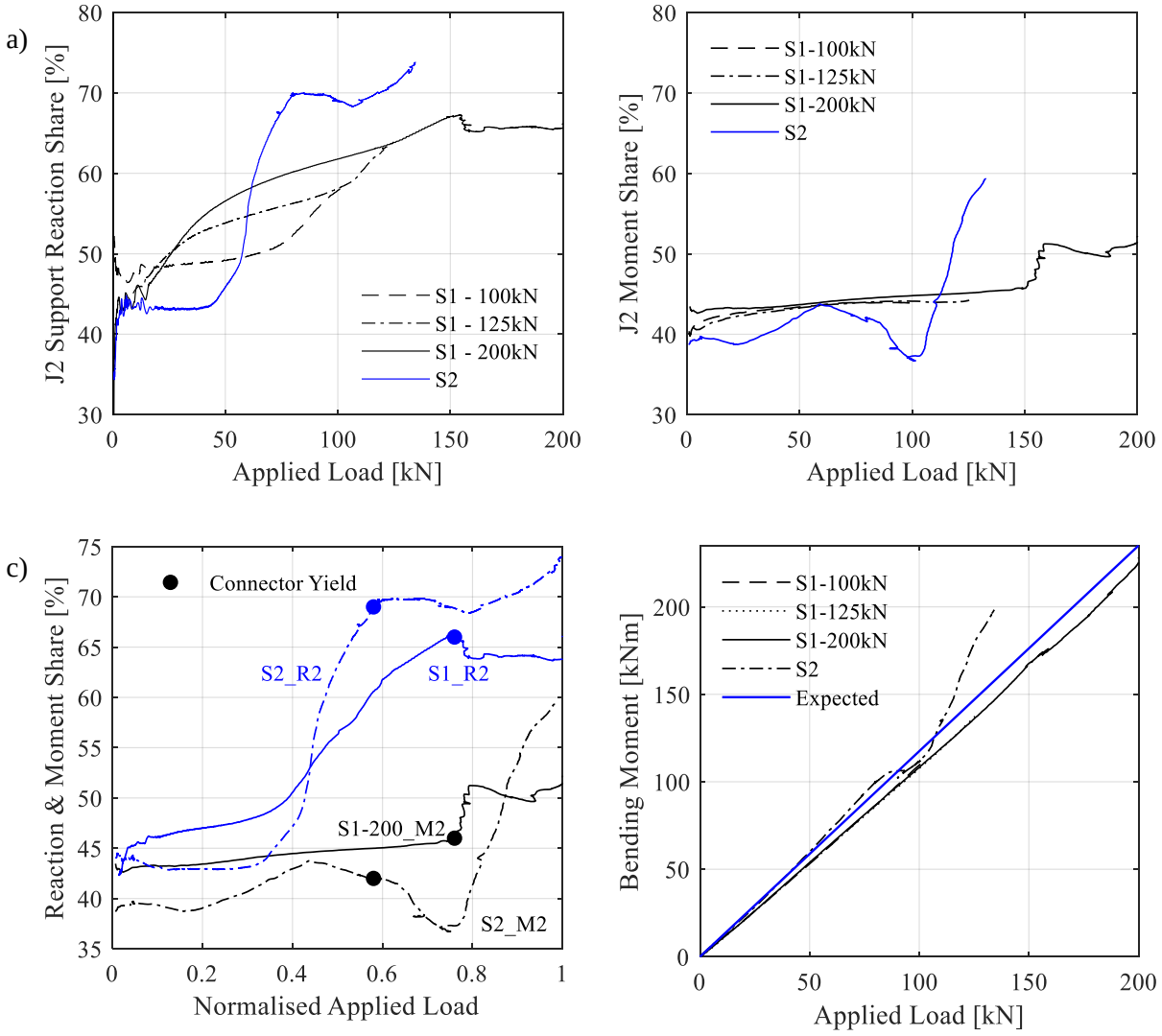

Figure 6 - (a) J2 support reaction share for tests on S1 and S2, (b) J2 bending moment share for tests on S1 and S2, (c) J2 bending moment and support reaction comparison normalised against peak load, and (d) actual bending moment values obtained from the analysis compared with the expected values based on equilibrium conditions

It is most instructive to compare results from the two specimens on the same axes to gain an understanding of the effect of altered connection design on load sharing across the specimens. Hence, Figure 6c presents results of the support reaction and bending moment sharing for the J2 T-sections of both S1 and S2. Assessing the load sharing between the two specimens in Figure 6c, there are some key points that can be inferred from the data:

- There is an abrupt increase in the J2 support reaction share of S2, occurring before the identified connector yield as marked on Figure 6c. The moment share for J2 increases also but at a later

point during the loading regime. This support reaction share is compared with a more gradual increase for S1, whilst still occurring primarily before connection yield.

- The reduction of connector density has had no adverse impact on the ability of the specimen to share bending moment. Whilst the moment sharing distributions may be less stable in S2 compared to S1, joist J2 has a lower share of the total bending moment until 86% of maximum applied load.
- The reduction of slab compressive strength has had no adverse impact on the ability of the specimen to share bending moment, however it has had a significant impact on the support reaction sharing (indicated in part by results from the nonlinear FE model which will be discussed later). This causes the disparities between transverse sharing of midspan moment and of support reaction to become even more pronounced: this reaches a maximum of 32% at 76% of peak applied load, compared 19.5% for S1.
- At high loads the moment sharing in both specimens becomes less favourable. This occurs at 76% of peak load for S1 and 79% for S2. These are both load levels where bangs were heard during testing (Figure 5) and could be representative of slab cracking in S1 and connector yield in S2.
- At failure the resultant reaction-moment sharing differences are similar (13% for S1, 14% for S2). The support reaction sharing remains in both cases the more adverse case, with 64% and 72% of the support reactions taken by the central joist for S1 and S2, respectively.

Figure 6d presents a comparison of the absolute values for the summed specimen section moment against applied load. The blue line in this figure represents the expected value based on equilibrium conditions. The excellent adherence of the summed moment profiles for both S1 and S2 to this expected value again signifies the reliability of this interpretation of the test data, and that the inferences made from the previous moment sharing and support reaction sharing relationships are credible.

Figure 7 and Figure 8 compare bending moment and support reaction sharing at specific points during the loading to failure tests, namely at the point shortly before each specimen experienced significant

nonlinear behaviour (see Figure 5), and shortly before failure. In addition to moment and support reaction, the deflection sharing has been included: whilst the summed midspan deflection of all three joists may not be considered a "total deflection", as joist deflections are independent in their own right, the purpose of including deflection sharing is to understand whether there are any relationships that can be derived between deflection and support reaction, or bending moment.

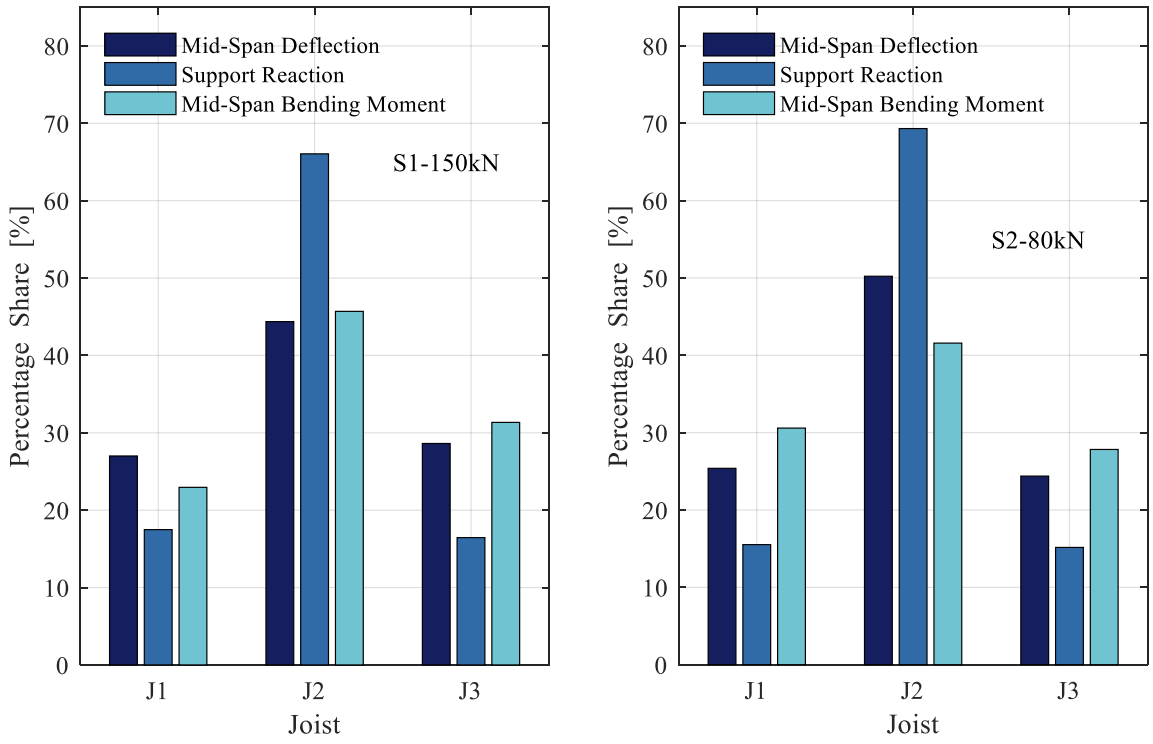

Figure 7 - Sharing profiles of deflection, support reaction, and bending moment for (a) S1, and (b) S2, at 20mm deflection

Figure 7 shows quite clearly that the bending moment distributions are much more favourable at 20mm deflection, and are in fact more favourable in specimen S2, compared with a less favourable support reaction sharing. In both cases the distributions of deflections match reasonably well with that of the bending moment distributions, especially in S1 where the differences are just 4%, 1%, and 3% for joists J1, J2, and J3 respectively. Comparing this with the failure sharing shown in Figure 8, some important distinctions may be made:

- Support reaction sharing is again less favourable than moment sharing, but the proportion of bending moment taken by joist two is greater than in Figure 7, resulting in a closer value to the support reaction sharing (difference of only 14% in S1 and S2).

- Deflection sharing on the whole matches more closely with support reaction sharing, and is the least favourable distribution in S2.
- All sharing distributions are less favourable in S2 compared to S1 at failure, leading to greater proportions of the deflection, support reaction, and bending moment being taken by the central joist J2.
- Both Figure 7 and Figure 8 highlight that the moment sharing is the least symmetric of all three metrics which have been assessed here.

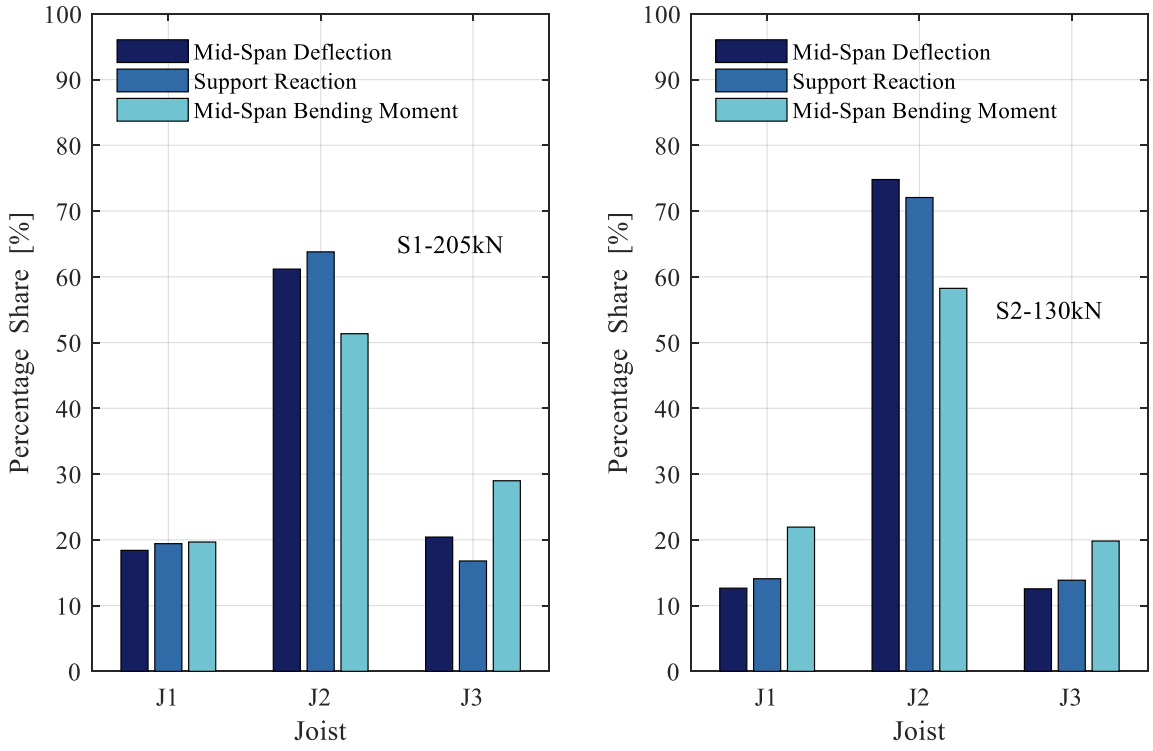

Figure 8 - Sharing profiles of deflection, support reaction, and bending moment at failure for (a) S1 at 205kN, and (b) S2 at 130kN

3.3 Full-Range Transverse Distributions of Deflection and Section Behaviours at Midspan

Further evidence as to the relative roles of cracking and connection yield may be seen in Figure 9 and Figure 10. Figure 9a presents deflection profiles for both specimens at 90% of their respective maximum applied loads. It suggests that a greater level of cracking in S2 compared with S1 allowed for a greater deflection of the middle joist compared to that of J1 and J3, whose deflections are of similar magnitudes. Note that the relative deflection of the central joist J2 compared with the average of J1 and J3, here termed the deflection ratio, is 5.1 for S2, compared to 2.8 for S1 highlighting the large impact that the increased level of cracking had on central T-section deflection.

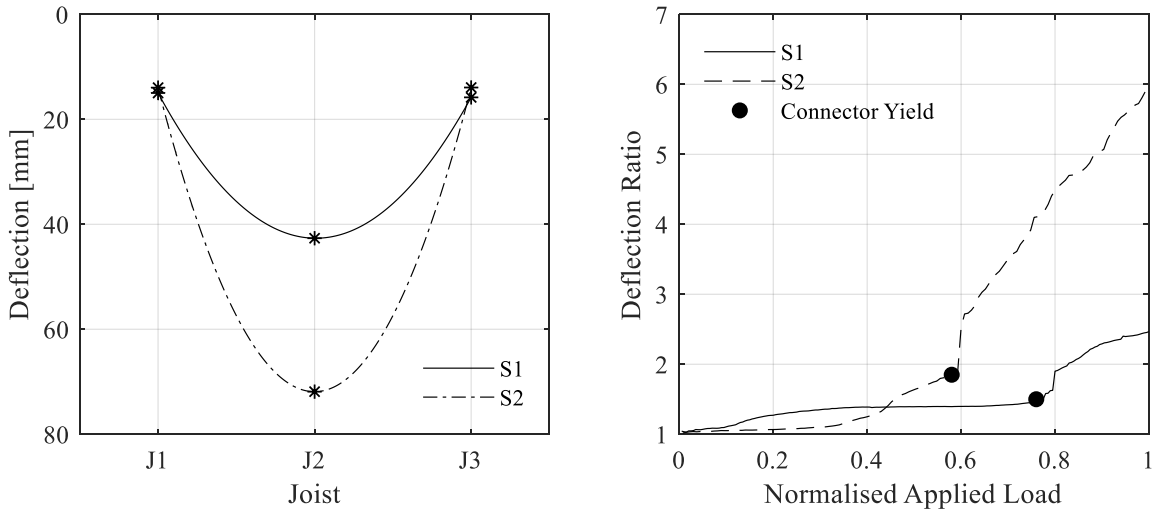

Figure 9 - (a) Joist midspan deflection at 90% of maximum applied load, and (b) J2 deflection ratio for all loads

Figure 9b examines the previously defined deflection ratio. In this plot, it can be seen that significant increases in the deflection ratio occur *after* the yielding of the mesh connectors, which in turn led to the sharp increase in J2 moment sharing as seen in Figure 6c.

Examining the through-joist strain distributions in Figure 9a and b, the slope for J2 is clearly distinct from both J1 and J3, which display near-symmetrical behaviour, a reflection of the good support conditions and experimental setup. Note also that at this point the neutral axis (zero-strain location) of the central joist is significantly lower than that of the outer joists, highlighting the moment of the J2 T-section well into the nonlinear regime as a result of significant connection yield.

Figure 10c highlights the position of the joist neutral axis across the loading spectrum for S1. Before connector yield occurs, the position of the neutral axis is relatively stable, indicating little slip between timber and concrete, reinforced by the slip data in Figure 5b, and therefore little influence of concrete cracking on specimen composite action. After connection yield, movement of the neutral axis of each joist occurs concurrently with the increase in deflection and curvature ratio. En-route to maximum load, the J2 neutral axis drops significantly and approaches the mid-depth of the joist (which would signify zero composite action), again reinforcing the conclusion of significant connector yield.

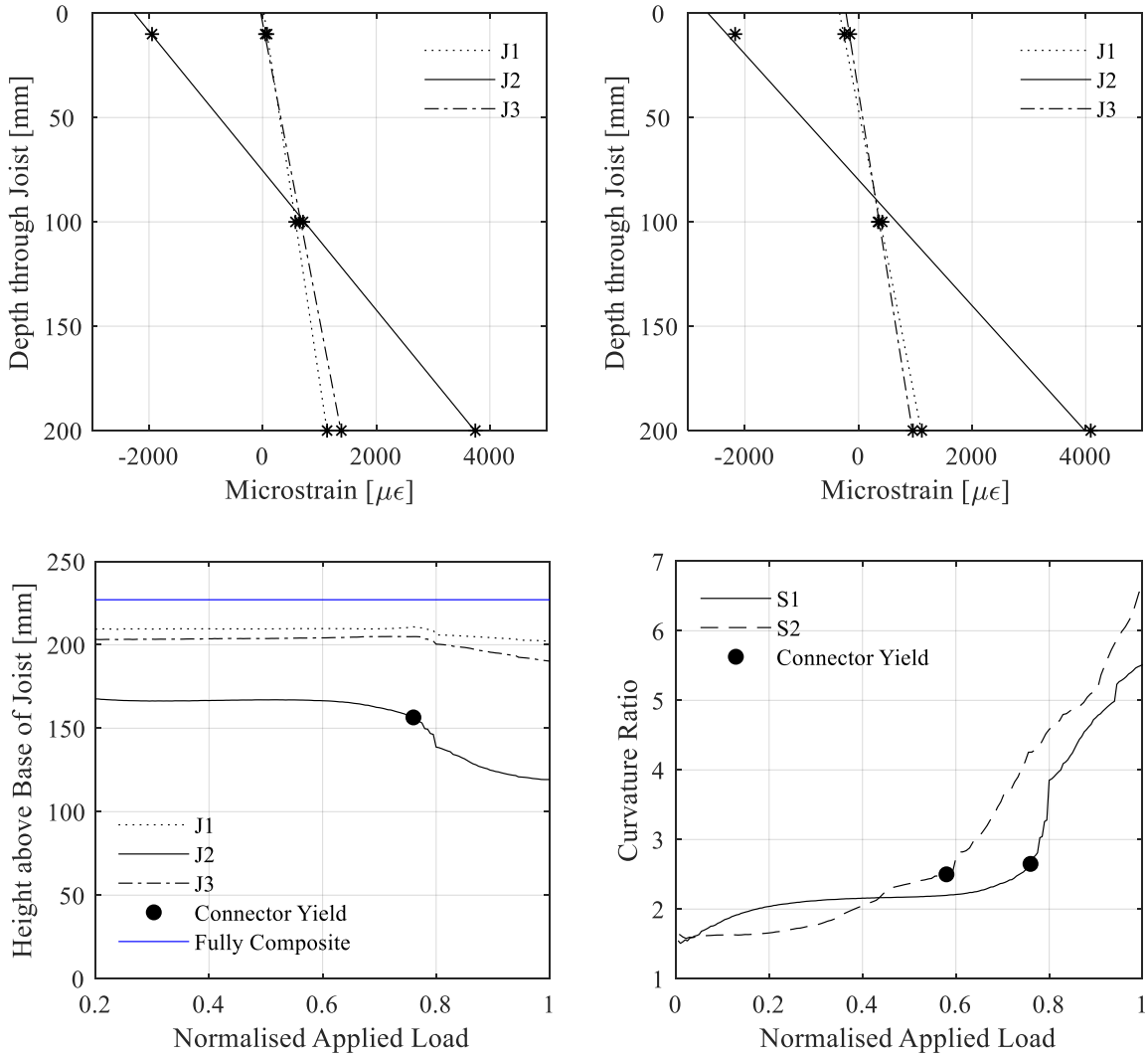

Figure 10 – Joist through-depth strain profiles at 90% of maximum applied load for (a) S1, and (b) S2, (c) neutral axis position of each timber joist in S1, and (d) J2 curvature ratio with respect to the average value of J1 and J3

Figure 10d presents the curvature ratio (namely the ratio of J2 curvature to the average curvature of J2 and J3). It shows similar trends to those displayed by the deflection ratio (Figure 9b). Note from both

Figure 9b and Figure 10c that the concrete cracking, which is demonstrably apparent *before* connection yield, has very little influence on the deflection or curvature ratio, highlighting the sensitivity of *moment sharing* to the occurrence of connector yield. Although the curvature ratio increased dramatically towards peak applied load, this does not translate directly to a seven-fold increase in moment due to the softening of the connections, and therefore introduction of significant slip strain at the timber-concrete interface.

The figures presented above enable the following conclusions to be drawn regarding the influence of concrete cracking and connection yield on the transverse load distribution response of the TCC specimen:

- Concrete cracking has a significant impact on the support reaction distribution within the TCC, but a relatively low impact on the bending moment distributions.
- Conversely, the yield of shear connectors has a profound impact on the bending moment and deflection distributions within the TCC, but do not affect the support reaction distributions as acutely.
- Therefore, if design for shear is required, concrete cracking must be investigated, and if design for moment is required, the connection yield must be fully understood.

3.4 Influence of Transverse Distribution on Failure Modes

The specimens underwent final failure in two different manners, outlined in Table 2, and it is thought that the difference for this is primarily due to the difference in concrete strength. S1 failed via a fracture of the underlying LVL joist J2 (Figure 11a), reaching maximum bending stress after continuing to deform significantly after reaching maximum load. This joist fracture immediately precipitated punching failure of the concrete slab along the centreline for approximately the central 60% of the span, which can be seen in Figure 12a. Note also in the figure the elliptical crack (outlined with the red dashes) which developed before the joist fracture. This was a result of the bowl-like deformations of the concrete, indicating a radial stress pattern in the slab.

Table 2 - Failure modes for specimens S1 and S2

Specimen	Failure Mode	
	Primary	**Secondary**
S1	Joist fracture (205kN)	Slab punching
S2	Slab punching	Joist fracture

Figure 11 – Primary failure modes of (a) specimen S1 (joist fracture), and (b) specimen S2 (concrete punching)

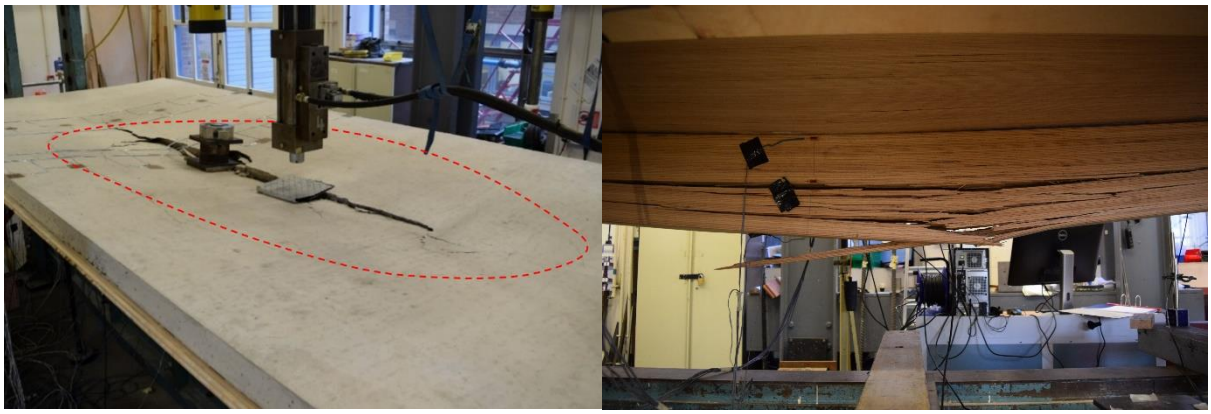

Figure 12 – Secondary failure modes of (a) specimen S1 (slab punching), and (b) specimen S2 (joist fracture)

Conversely, S2 failed due to a punching failure of the concrete slab (pictured in Figure 11b), which subsequently led to the fracture of joist J2 shortly afterwards (Figure 12b), as the concrete slab was providing a significantly reduced structural capacity and therefore the joist alone was now supporting the majority of the applied load. Despite a similar deflection profile, the elliptical cracks that developed in S1 were not present in S2. The longitudinal crack that resulted from the punching failure was significantly greater in length (approx. 80% of span) compared to S1, indicating this as the primary failure mode.

4 Nonlinear Finite Element Validation

In order to determine that the results obtained from the two experimental specimens are predictable, a finite element (FE) model was developed using Abaqus FEA, developed by ABAQUS Inc. [n]. Figure 13a presents an expanded overview of the model highlighting the key mechanical features used. The concrete slab and timber joists, alongside the support blocks and loading plate, were made using solid brick elements, type C3D8R, which consist of 8 nodes with reduced integration and hourglass control.

The timber was specified as orthotropic using manufacturer provided material properties where possible [r]. The mean elastic modulus in the major axis was specified as 16.7 GPa. For the concrete, elastic moduli of 34 GPa and 31 GPa ere specified for specimens S1 and S2 respectively, alongside compressive and tensile strengths of 43 MPa, 3.3 MPa - S1 and 33 MPa, 2 MPa - S2. In addition, a concrete damaged plasticity model was used to represent the constitutive behaviour of the concrete once either cracked or within its highly nonlinear compressive regime. In order to model the expanded mesh plate shear connection in this arrangement, axial connector elements were utilised, and provided with a nonlinear shear force-slip profile. This shear force-slip profile was fed into the model as a set of data points obtained from experimental testing as mentioned previously in the paper, and may be seen in Figure 13b. The profile used is the average slip profile from the four tests conducted. Analyses which used the minimum and maximum envelopes of slip behaviour did not differ significantly from the average value and so are not presented. In addition to the use of axial connector elements to model the

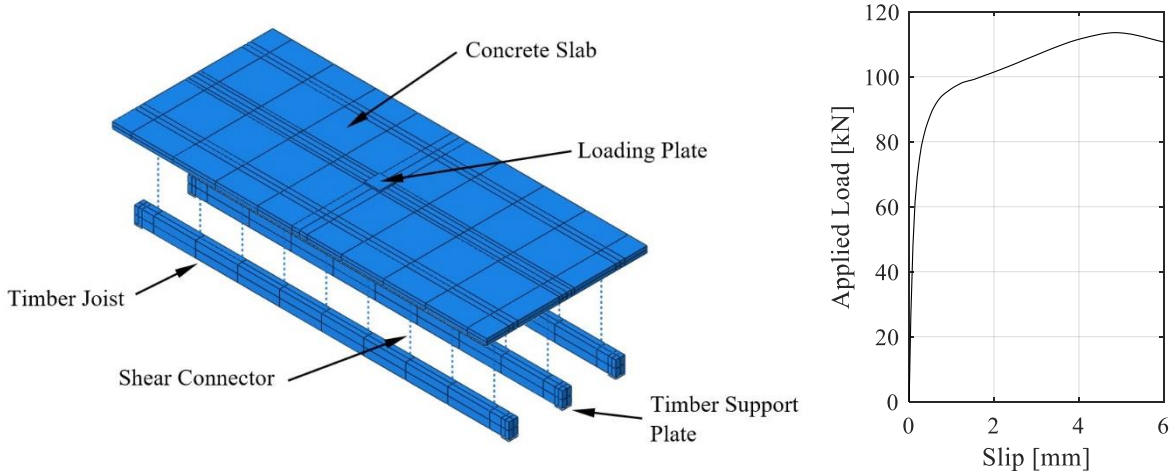

Figure 13 – (a) 3D finite element model produced in Abaqus FEA, and (b) connector stiffness profile used in analysis

longitudinal slip stiffness of the connections, two further connectors were positioned at each connector location to model the transverse and vertical stiffness of the connectors, as done previously by Chiorean and Buru [s] and Classen [t]. It was assumed in this model that there was no separation of slab from joist, and no transverse relative horizontal slip. Therefore, these transverse and vertical connections were provided with a high linear stiffness.

Nonlinear effects from large displacements were taken into account using the nlgeom feature in Abaqus, utilising a load control regime to converge at each step. The step size was defined to be 20kN, with the initial increment of this step set as 0.1 (2kN), and the analysis was terminated if convergence at each step could not be achieved in 100 iterations. The 0.1 step increment size was appropriate during the linear and early nonlinear regime, however smaller increments (down to 0.01 for S1 and $5x10^{-6}$ for S2) were required towards the maximum applied load.

4.1 Analysis Results

The results from the analysis show that the predicted and experimental load vs. deflection (Figure 14), and support reaction vs. load (Figure 16) plots agree well for both specimens. This is especially the case for the linear and early nonlinear regimes. While the experimental observations and results indicate that cracking of the concrete and yield of the connections occurred, the FEA predicted significant cracking of the slab but no yield of the connections (Figure 15). The peak FE-predicted connection force was 72% of the connection yield load, so the analysis approached, without activating yield. Hence the nonlinearities evident on the predicted responses are due to concrete slab cracking.

Examining the results in more detail, Figure 14a shows that the FE model estimated the deflections with reasonable accuracy up to 80kN for both specimens. The experimental results show initially linear behaviour, then some nonlinearity just before first yield of the connections, and then a significant and abrupt lowering of the gradient brought about by yield. The FE predictions are seen to agree with the experiments in linear behaviour at low loads, then increasing evidence of nonlinearity due to progressive cracking of the concrete, but the predicted results never show the abrupt lowering of load-deflection gradient at any stage because no connection yield is predicted by the FEA.

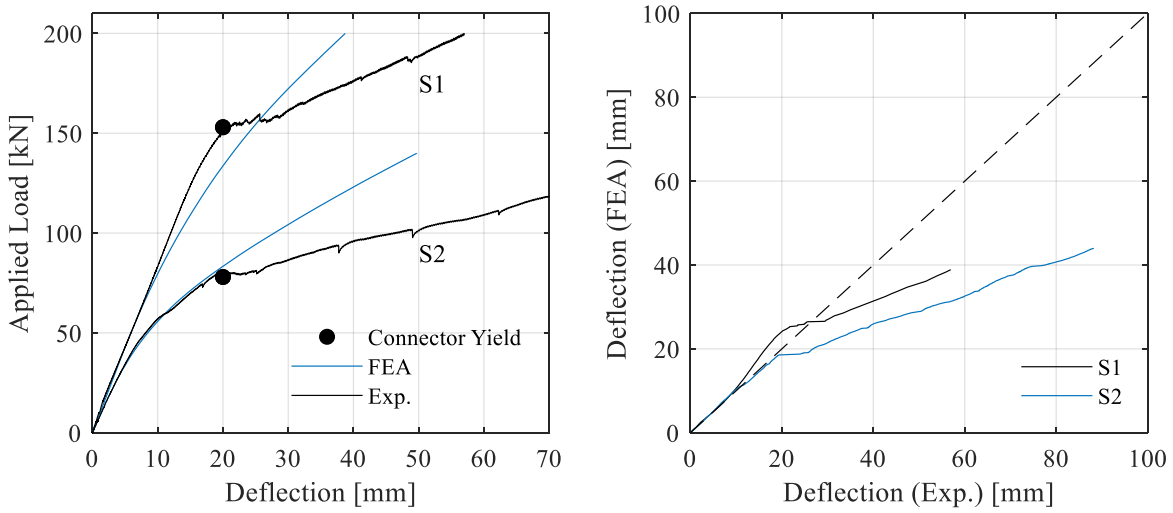

Figure 14 – numerical and experimental comparisons for (a) applied load vs. deflection of J2, and (b) deflection comparisons for J2

Figure 14b presents a comparison of model and experimental deflection for both specimens: S1 shows excellent agreement up to 28mm displacement, and 19mm for S2. The deviation between experimental and numerical models was calculated by means of the square root of the sum of the squares method (SRSS). In this case, the difference between the deflections was calculated at each loading increment. Up to the point of nonlinearity (155kN for S1, and 80kN for S2), the SRSS divergence is 15 for S1 and 8 for S2, reinforcing this excellent pre- yield agreement. Over the whole loading regime, these ratios increase to 62 and 445 respectively, highlighting the better performance overall of the model against S1 than for S2, but the better representation of reality of S2 up to the point of nonlinearity.

The measured and predicted specimen load vs. connection slip responses are compared in Figure 15. The slip profiles shown are those of connectors 2 and 8 in S1, and 2 and 4 in S2 (shown in Figure 1), in

each case with the chosen pair being symmetrically distributed about midspan of the specimen. Hence that the experimental data of Figure 15 show very similar load-slip curves within each pair, suggesting a longitudinally symmetric load response within each of S1 and S2. It may be seen that within the linear experimental regime before connector yield, both models show good agreement. The FE model did not predict the yield of the connectors, characterised by a sudden increase in slip with respect to applied load, and therefore there is divergence between the predictions and the experimental findings after this point. The fact that the yield was not predicted highlights that any manifestation of nonlinearity in the FE predictions was due to concrete slab cracking.

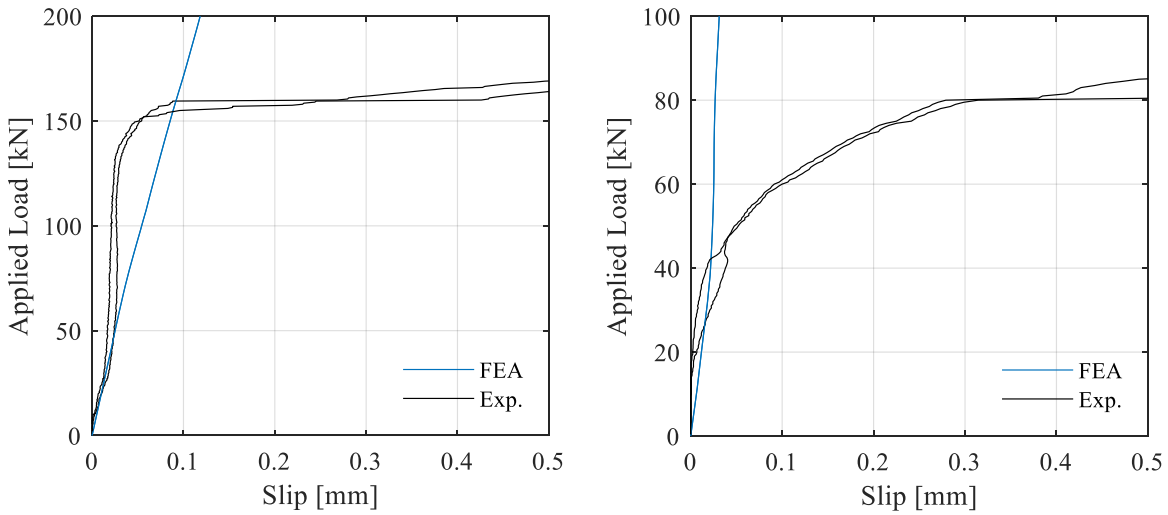

Figure 15 – connector slip in (a) S1, connectors 2 and 8, and (b) S2, connectors 2 and 4

The prediction of J2 support reaction with increasing load, shown in Figure 16a, was consistently in good agreement with the experimental results. The close agreement for the support reaction sharing for both S1 and S2 may be seen in Figure 16b. Over the entire loading regime, the deviation from experimental to numerical results, again calculated using the SRSS method, is 84 for S1, and 231 for S2. This is indicative of the better overall agreement for S1, especially as it approaches maximum load where it tends back towards excellent agreement. If the divergence is calculated from zero load up to the point where the model begins to experience a shift towards J2 taking increasing load (72kN for S1, 57kN for S2), the deviations become 68 and 7, respectively, once again highlighting the better agreement of S2 at lower loads.

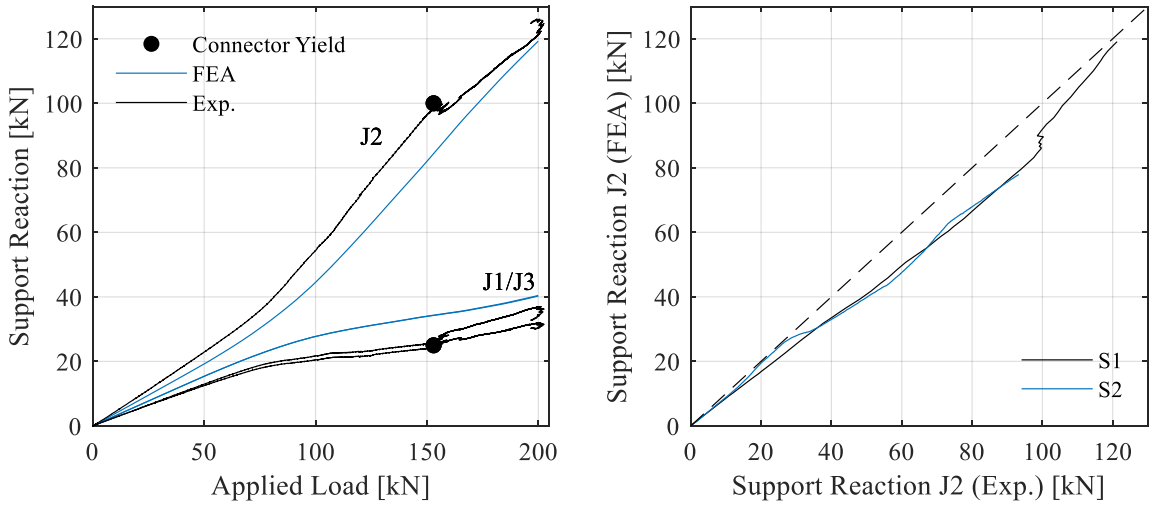

Figure 16 – (a) support reaction vs. applied load for S1, and (b) experimental and numerical support reaction comparisons for J2, both specimens

Important to note here is that after the point of experimental connector yield the agreement between predicted and experimental support reactions increases up towards failure. This indicates that the yielding of the connectors affects the deflection much more acutely than that of the support reactions, which are more a function of the transverse stiffness and load distribution within the specimen.

Figure 17 shows experimental and predicted stresses at the soffits of the central joists J2 for both specimens. Again, at loads up to 80kN there is excellent agreement between the FEA models and the experimental data. After this, the agreement remains good for both specimens. At maximum load the soffit stresses are 62MPa and 59MPa for S1 and S2 respectively, which are both approaching the manufacturer-stated capacity of the timber. Recall that each specimen failed shortly after reaching these maximum loads and so the stress would be expected to increase further.

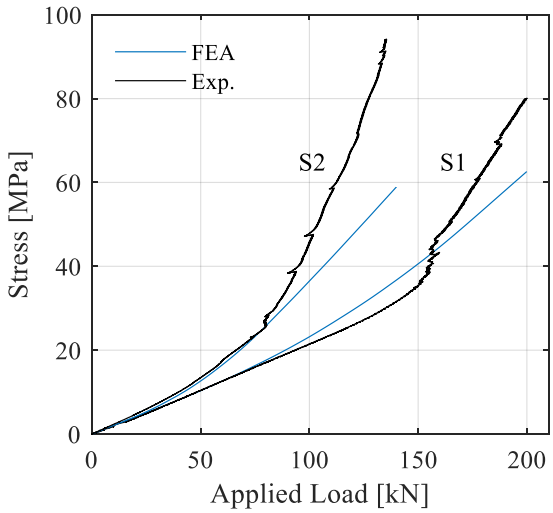

Figure 17 - joist soffit stresses compared for experimental and FE models

The results of the FE analysis provide confidence that the behaviour of the experimental specimens during the linear regime may be estimated with a high degree of confidence, and that the concrete slab plays a significant and continuing role in the transverse distribution behaviour of the modelled TCC specimens beyond the experimental connection yield. Given that the connectors are not able to yield in the FEA model, a significant proportion of the specimen behaviour is dependent on the nonlinear behaviour of the concrete slab. Whilst this result has proved useful in identifying the continuing influence of concrete cracking on the nonlinear behaviour of the specimen following connector yield, further work should be done to investigate the impact of tri-axial shear connector behaviour to determine whether this might improve the accuracy of the FEA results.

4.2 Concrete Strength Influence

As part of a larger sensitivity study, the influence of the concrete grade on the share of the support reaction taken by the central joist J2 was investigated. Figure 18a shows the changes to the J2 support reaction share profile as the concrete grade was altered in specimen S1. The relation to the concrete grade of the specified tensile strength and elastic modulus, as defined in Eurocode 2 [q], are shown in Figure 18b. The plots of Figure 18a show the following important trends:

- At low load, before any concrete cracking occurs, the elastic state of the structure is constant and so the J2 reaction share remains constant with load increase. At this stage the share drops slightly as concrete strength increases, because the associated increased transverse stiffness of the slab transfers slightly more of the load to J1 and J3.
- After this initial constant share phase, the J2 reaction share increases dramatically with further load increase. This is due to cracking of the slab, causing the slab's transverse stiffness to drop, and which in turn causes the slab to transmit less of the applied load on the specimen to J1 and J3, hence more of the load is taken up by J2.
- Towards the peak loads, the reaction share taken by J2 begins to level off. This is very likely because a lot of cracking has already occurred by then, so not much further cracking can occur, hence the transverse stiffness profile of the slab and with it the share of the support reaction have levelled off.
- Throughout the nonlinear regime, the higher concrete strengths lead to persistently smaller J2 reaction shares, owing presumably to the lesser extents of cracking and so to stiffer transverse slabs which transmit more of the applied load to J1 and J3, leaving J2 with less reaction share.

- The validated FEA shows that increasing the concrete grade from RC20 to RC50 causes a predicted 12.5% drop in support reaction share for the central TCC T-section at 50% of the peak applied load, because the progressively stiffening slab (with increased concrete grade) transmitted more of the applied load to the transversely neighbouring TCC T-sections.

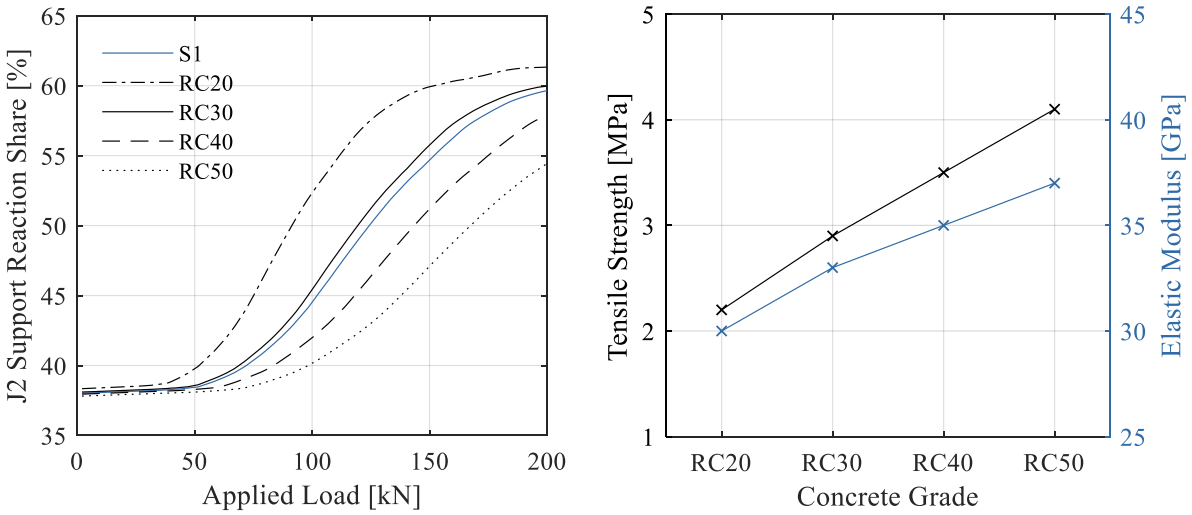

Figure 18 – (a) Influence of concrete grade on J2 support reaction share with increasing applied load (S1), and (b) tensile strength and elastic modulus values associated with each concrete grade [q]

5 Conclusions

This paper presents the results of a new analysis into the results of two experimental multi-joist timber-concrete composite floor specimens, with intentionally differing connection layouts, and inadvertently differing concrete strengths. A newly developed FE model was then used to gain further insight into the experimental results. The primary conclusions that have been drawn by this paper are:

- The present multi-joist TCC floor specimens under concentrated loading exhibited three key stages of behaviour: a period of linear behaviour; a period of nonlinearity characterised by a shifting of reaction to the central joist at the supports due to concrete cracking; and a further period of nonlinearity due to longitudinal shear yield of the connections.

- When provided in a suitable arrangement, the steel expanded mesh shear connector undergoes significant ductile behaviour which in turn allows the structure to experience a greater level of deformation before brittle failure. A denser arrangement can be used to increase the maximum load of the specimen albeit at a lower deflection.
- Whilst the connection yield had a significant impact on the global specimen deflections, it was the nonlinearities due to concrete cracking which influenced the support reaction and bending moment distributions to a significant degree.
- Bending moment sharing between joists is more favourable than support reaction sharing, even when a reduced shear connection density is provided in the structure, thus reducing the longitudinal section stiffness.
- The sensitivity of bending moment sharing to reduced connector density and reduced concrete compressive strength is significantly less than that of the support reaction sharing.
- The developed full 3D FEA model can predict the behaviour of the specimens with confidence. It demonstrated a decrease of 12.5% in central TCC T-section support reaction share at 50% peak applied load when the concrete grade was increased from RC20 to RC50, because the progressively stiffening slab (with increased concrete grade) was able to transmit more of the applied load to the transversely neighbouring TCC T-sections.

Further experiments to continue to increase the available test data on full-scale TCC floors will help to contribute towards an increasing understanding of this system of construction and enable more efficient design of these structures to underpin their more widespread use. Investigating the impact of changes in the shear force-slip profile, and tri-linear behaviour, of the connections in the nonlinear FE model will enable further accuracy improvements to be obtained.

6 References

[j] Deam, B. L., Fragiacomo, M., Buchanan, A. H., (2008) 'Connections for composite concrete slab and LVL flooring systems' Materials and Structures **41** pp. 495-507.

[n] Frangi, A., Fontana, M., (2003) 'Elasto-Plastic Model for Timber-Concrete Composite Beams with Ductile Connection' Structural Engineering International **1\2003** pp. 47-57.

[b] Lukaszewska, E. (2009) 'Development of Prefabricated Timber-Concrete Composite Floors' Thesis, Lulea University of Technology.

[c] Pault, J. D. and Gutkowski, R. M. (1977) 'Composite action in glulam timber bridge systems' Report, Colorado State University.

[o] Monteiro, S. R. S., Dias, A. M. P. G., Negrao, J. H. J. D., (2010) 'Experimental and numerical evaluation of notched timber-concrete joints mechanical behaviour' Proceedings of the 11th World Conference on Timber Engineering, Riva del Garda, Italy.

[l] Boccadoro, L., Zweidler, S., Steiger, R., Frangi, A., (2017) 'Analysis of shear transfer and gap opening in timber– concrete composite members with notched connections' Materials and Structures **50** pp. 1-15.

[k] Tannert, T., Endacott, B., Brunner, M. and Vallée, T., (2017) 'Long-term performance of adhesively bonded timber-concrete composites' International Journal of Adhesion and Adhesives, **72**, pp.51-61.

[a] Brunner, M., Romer, M. and Schnüriger, M., (2007) 'Timber-concrete-composite with an adhesive connector (wet on wet process)' Materials and Structures, **40**(1), pp.119-126.

[g] Bathon, L. A., Clouston, P., (2004) 'Experimental and numerical results on semi prestressed wood-concrete composite floor systems for long span applications' Proceedings of the 8th World Conference on Timber Engineering, Lahti, Finland.

[h] Clouston, P., Bathon, L. A., Schreyer, A., (2005) 'Shear and Bending Performance of a Novel Wood–Concrete Composite System' Journal of Structural Engineering **131**(9) pp. 1404-1412.

[i] TICOMTEC (2019). 'HBV References' [online] TICOMTEC. Available at: https://ticomtec.de/en/hbv-systems/referenzen-hbv/ [Accessed 16 Jul. 2019].

[p] Sebastian, W. M., Mudie, J., Cox, G., Piazza, M., Tomasi, R., Giongo, I., (2016) 'Insight into mechanics of externally indeterminate hardwood–concrete composite beams' *Construction and Building Materials* **102**(2) pp. 1029-1048.

[d] Monteiro, S. R. S., Dias, A. M. P. G., and Lopes, S. M. R. (2016). 'Transverse distribution of internal forces in timber-concrete floors under external point and line loads' Construction and Building Materials, **102**:1049–1059.

[e] Kieslich, H., Holschemacher, K., (2016). 'Transversal load sharing in timber-concrete floors - experimental and numerical investigations' *Proceedings of the 14th World Conference on Timber Engineering*, Vienna, Austria.

[f] Mudie, J., Sebastian, W. M., Norman, J., Bond, I., (2019) 'Experimental study of Moment sharing in Multi-Joist Timber-Concrete Composite floors From Zero Load Up To Failure' Construction and Building Materials, **225**, pp. 956-971.

[m] British Standards Institution, (2004) 'BS EN 1995-1-1:2004. Eurocode 5: Design of timber structures — Part 1-1: General — Common rules and rules for buildings' London, British Standards Institution.

[q] British Standards Institution, (2004) 'BS EN 1992-1-1:2004. Eurocode 2: Design of concrete structures — Part 1-1: General — Common rules and rules for buildings' London, British Standards Institution.

[r] Pollmeier GmbH, (2015) 'BauBuche Declaration of Performance GL70' Germany, Pollmeier.

[s] Chiorean, C. G. and Buru, S. M., (2017). 'Practical nonlinear inelastic analysis method of composite steel-concrete beams with partial composite action' *Engineering Structures*, **134**:74–106.

[t] Classen, M., (2018). 'Limitations on the use of partial shear connection in composite beams with steel t-sections and uniformly spaced rib shear connectors' *Journal of Constructional Steel Research*, **142**:99–112.